Regular and chaotic dynamics of optically pumped molecular lasers

J. V. Moloney, W. Forysiak, J. S. Uppal, and R. G. Harrison
Department of Physics, Heriot-Watt University, Edinburgh EH14 4AS, United Kingdom
(Received 19 January 1988; revised manuscript received 15 June 1988)

We present a detailed analysis of the dynamical behavior of an optically pumped molecular laser. This study combines bifurcation and power spectral analysis with numerical investigation of the global features of attractor topology under control parameter variation. The special role of the pump laser in generating physically distinct periodic and chaotic dynamics is emphasized through the complementary use of laser gain and dispersion characteristics. Our main results are the following: (i) instabilities associated with the physically distinct mechanisms of relaxation and pump-induced Rabi sideband oscillations are readily generated; (ii) the topological characteristics of both periodic and chaotic attractors reflect these physically distinct mechanisms, making it possible to discriminate between both types of behavior in heterodyne power spectra; and (iii) the ratio of deenergization to dipole-dephasing rates is central to determining the operating characteristics of the laser.

I. INTRODUCTION

The subject of laser instabilities began with the first observation of lasing emission itself in the early 1960s.[1] Generally, spontaneous pulsations in lasers have been considered undesirable, and except for special applications such as mode locking or Q switching, significant effort has been made to stabilize commercial lasers against oscillation. The realization in the early 1980s that many of the observed phenomena may be manifestations of chaotic behavior led to a renewed theoretical and experimental effort over a broad front. It is now well established that many laser systems exhibit chaotic dynamics over a wide range of operating conditions.

The simplest conceivable laser model is a single-mode homogeneously broadened laser. In 1975 Haken demonstrated that the Maxwell-Bloch equations describing such a laser are isomorphic to the much studied Lorenz equations modeling turbulent flow in fluids.[2] The Lorenz equations were known to exhibit a great variety of dynamical behavior over a wide range of parameter values. It was quickly realized, however, that the operating conditions necessary to observe the predicted chaotic behavior in these lasers, namely, bad cavity conditions and pumping at more than nine times above threshold,[2,3] were physically unrealistic. Meanwhile, chaotic behavior has been relatively easy to observe in homogeneously broadened lasers under single-mode operation with external modulation or under multimode operation. Additionally, detailed experimental and computational studies of inhomogeneously broadened lasers have established that such systems show chaotic behavior close to the lasing threshold. Recent developments on laser instabilities are reviewed in Refs. 4–14.

Optically pumped molecular lasers (OPML's) have emerged recently as promising candidates for the observation of chaotic dynamics in a single-mode homogeneously broadened laser system. The semiclassical Maxwell-Bloch equations describing optically pumped amplifier systems have been studied extensively in the literature.[15–20] More recently these treatments have been extended to describe laser oscillators.[20–27] Efforts have been made to truncate the set of ten ordinary differential equations (ODE's) by the adiabatic elimination of fast variables. Thus, conditions for the reduction of the equations to the three-equation Lorenz-Haken model have been identified[21] and a four-equation version has been studied which predicts instabilities as low as 1.6 times above the lasing threshold.[24] Experimental evidence of Lorenz-like and still more intricate bifurcation structures has already been reported.[28,29]

In this article we study the full OPML model for conditions of resonant pumping with resonant lasing emission. The cavity loss and laser gain are held constant and our primary control parameter is the pump laser amplitude. Assuming the deenergization and dipole dephasing rates to be the same for each of the three levels, we use their ratio $b=\Gamma/\gamma$ as our secondary bifurcation parameter; whether the laser exhibits steady, pulsing, or chaotic behavior depends critically on this ratio. The bifurcation analysis isolates branches of periodic solutions which, through the complementary use of gain and dispersion curves, can be associated with the physically distinct mechanisms of sustained relaxation oscillation and pump-induced Rabi sideband oscillation.[25] These separate periodic branches strongly influence the attractor topology within the chaotic parameter window where the physical mechanisms strongly interact. We show that heterodyne power spectra can distinguish between dynamical motions associated with these two physical mechanisms, whether periodic or chaotic. Lyapunov exponents are calculated using an algorithm due to Wolf and Swinney[30] that confirm a low-dimension chaotic behavior further supported by attractor pictures. Our limited bifurcation analysis suggests the existence of higher codimension bifurcations. This important question remains to be addressed before a relatively complete pic-

ture of the dynamical behavior of the OPML can be fully ascertained.

II. THEORY AND BIFURCATION ANALYSIS

A schematic diagram of the three-level OPML is shown in Fig. 1. An external pump of amplitude α selectively excites level 2 which acts as the upper level for the lasing transition $2\rightarrow 3$. The coherent pumping of level 2 is particularly important as it can significantly alter the gain and dispersion characteristics seen by the lasing emission field β. Specifically, the conventional homogeneously broadened gain curve can be Rabi split by the saturating pump, leading to an inverted gain distribution at line center. Consequently, the dispersion characteristic seen by the lasing emission can be strongly distorted. The result is a potentially unstable single-mode laser in the vicinity of its natural relaxation oscillation frequency, manifested as sustained relaxation oscillations or chaotic emission dependent on the pump strength. Additionally, under stronger pumping conditions more than one frequency can be resonant with the single-mode cavity making possible Rabi oscillation with a frequency proportional to the effective Rabi frequency of the pumping transition. For the laser parameter values chosen here the physical processes arising from both relaxation oscillations and Rabi splitting can occur and overlap within a pump control parameter window. In other circumstances either process may appear in isolation. Furthermore, period-doubling cascades to chaotic attractors may occur on either physical branch of periodic solutions when the cavity loss is close to the good cavity boundary $\sigma=1+b$. Our numerical studies indicate that the bad cavity condition $\sigma>1+b$ does not need to be satisfied for chaotic dynamics, and moreover, that the restrictive condition of pumping at more than nine times above threshold, necessary for the Lorenz-Haken system, does not apply to this OPML model.

The OPML equations are a straightforward generalization of the usual semiclassical system of Lamb[31] to a three-level model. These are

$$\begin{aligned}
\dot{\beta}&=-(\sigma\beta+ig\rho_{23})\ ,\\
\dot{\rho}_{21}&=-(1-i\delta_p)\rho_{21}+i\alpha D_{21}-i\beta\rho_{31}\ ,\\
\dot{\rho}_{23}&=-(1-i\delta_s)\rho_{23}+i\beta D_{23}-i\alpha\rho_{31}^*\ ,\\
\dot{\rho}_{31}&=-[1+i(\delta_p+\delta_s)]\rho_{31}-i\beta^*\rho_{21}+i\alpha\rho_{23}^*\ ,\\
\dot{D}_{21}&=-b(1+D_{21})-4\,\mathrm{Im}(\alpha^*\rho_{21})-2\,\mathrm{Im}(\beta^*\rho_{23})\ ,\\
\dot{D}_{23}&=-bD_{23}-2\,\mathrm{Im}(\alpha^*\rho_{21})-4\,\mathrm{Im}(\beta^*\rho_{23})\ .
\end{aligned}\tag{2.1}$$

Here β refers to the lasing emission magnitude and is complex, in general, ρ_{ij} are the off-diagonal density-matrix elements for levels i and j, D_{ij} the population inversion $(\rho_{ii}-\rho_{jj})$ between respective levels, and δ_p (δ_s) refer to the detuning of the pump (signal) from resonance. The laser control parameters are σ, the cavity damping constant; g, the unsaturated gain; α, the pump laser amplitude; and $b=\Gamma/\gamma$, the ratio of deenergization to dipole dephasing rates. All parameters and the time t are scaled to the dipole dephasing width γ.

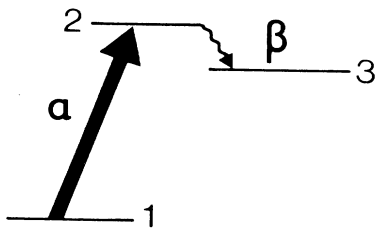

FIG. 1. Schematic of a coherently pumped three-level OPML.

Upon specializing to resonant pumping ($\delta_p=0$) and resonant lasing emission ($\delta_s=0$) the above set of ten coupled ODE's reduces to the following set of six equations:

$$\begin{aligned}
\dot{x}_1&=-\sigma x_1+gx_3\ ,\\
\dot{x}_2&=-x_2-x_1x_4+\alpha x_5\ ,\\
\dot{x}_3&=-x_3+x_1x_6-\alpha x_4\ ,\\
\dot{x}_4&=-x_4+x_1x_2+\alpha x_3\ ,\\
\dot{x}_5&=-b(1+x_5)-2x_1x_3-4\alpha x_2\ ,\\
\dot{x}_6&=-bx_6-4x_1x_3-2\alpha x_2\ ,
\end{aligned}\tag{2.2}$$

where the real variables x_i correspond to the physical variables as follows: $x_1\equiv\mathrm{Re}\beta$, $x_2\equiv\mathrm{Im}\rho_{21}$, $x_3\equiv\mathrm{Im}\rho_{23}$, $x_4\equiv\mathrm{Re}\rho_{31}$, $x_5\equiv D_{21}$, and $x_6\equiv D_{23}$. This set of six ODE's is the focus of the following bifurcation and numerical analysis. The laser gain and dispersion curves are generated from the known steady-state solutions to Eqs. (2.1).[20] The steady-state solutions to the set (2.2) are straightforward to derive. Here we require only the steady-state solution for the nonlasing branch,

$$x_1^0=0,\quad x_2^0=-\frac{\alpha b}{b+4\alpha^2},\quad x_3^0=x_4^0=0\ ,$$
$$x_5^0=-\frac{b}{b+4\alpha^2},\quad x_6^0=\frac{2\alpha^2}{b+4\alpha^2}$$

which is used to start the path-following procedure of the bifurcation package.[32]

By setting $\sigma=10$ and $g=50$, we use the pump laser amplitude α as our primary control parameter. Figure 2 captures the laser-operating characteristics under pump variation for a range of values of b. Solid and dashed curves in each diagram refer to branches of stable and unstable steady-state solutions, respectively. Branches of stable and unstable periodic solutions are represented by closed and open circles, respectively.

The operating characteristic of the OPML is simplest for $b=1.0$ [Fig. 2(a)]. When α is small, the nonlasing branch ($\beta=0$) of stationary solutions is stable and there is no lasing emission. At BP1, which marks the first laser threshold, a pitchfork bifurcation occurs to a steady lasing state ($\beta\neq 0$). As the pump amplitude is then increased, the lasing emission strength grows, reaches a

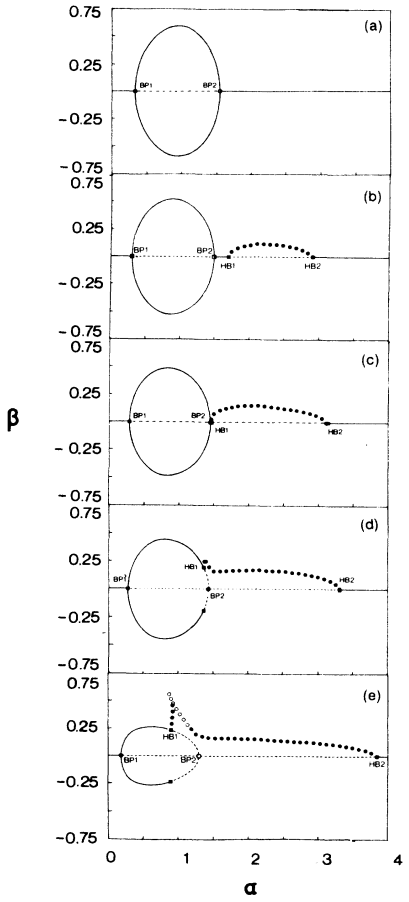

FIG. 2. Bifurcation diagrams for $b=1.0,0.8,0.7,0.6,0.2$[(a)–(e)]. Plots show laser emission amplitude β vs pump amplitude α. Solid lines denote branches of stationary solutions, dashed lines denote unstable stationary solutions. Closed and open circles mark the maximum amplitudes of branches of stable and unstable periodic solutions, respectively. Open squares represent pitchfork bifurcation points, whereas closed squares represent Hopf bifurcation points (labeled BP and HB).

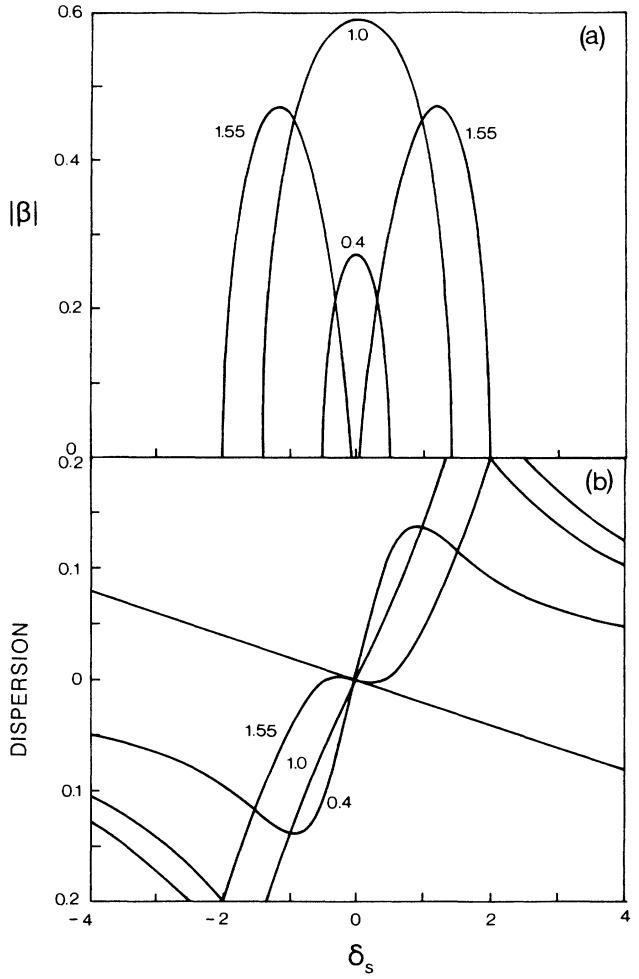

FIG. 3. Variation of the laser emission amplitude β (a) and cavity dispersion (b) with laser signal detuning for $b=1.0$. For $\alpha=0.4$ and 1.0, the laser is above the lasing threshold and the corresponding dispersion relation has a single intersection with the cavity line at the line center. At $\alpha=1.55$ the center of the emission line drops below lasing threshold and lasing ceases.

maximum value, and then decreases. Lasing ceases at the second pitchfork bifurcation point BP2, beyond which no further lasing action occurs. This behavior can be understood physically by examining the gain and dispersion characteristics seen by the lasing emission (Fig. 3). The leveling off and subsequent reduction in lasing strength is a consequence of the pump laser α inducing a Rabi splitting of the levels 1 and 2. As the degree of Rabi splitting grows, the center-line emission decreases in magnitude and lasing ceases when center-line gain drops below threshold. Figure 2 shows the start and end points of the steady-state lasing branches to be relatively insensitive to parameter b. The variation in strength of the lasing emission with parameter b can be understood from the following simple physical argument. The rate of removal of population from the lower lasing level 3 is strongly dependent on the deenergization rate Γ, whereas the upper lasing level population is relatively insensitive to Γ because of the saturating pump. Consequently, as $b \rightarrow 1$, population is removed more rapidly from the lower lasing level and the net inversion increases resulting in a stronger emission field.

A new feature appears for $b=0.8$ [Fig. 2(b)] where a branch of stable periodic solutions appears on the nonlasing branch between the Hopf bifurcation points, HB1 and HB2. This corresponds to the spontaneous appearance of regular pulsations from an initially nonlasing state. These periodic solutions can be identified with pump-induced Rabi sideband oscillations by referring to the gain and dispersion characteristics shown in Fig. 4. The initial Hopf bifurcation at HB1 coincides precisely with the point at which new intersections appear between the strongly distorted dispersion curve and the straight cavity line which determines the laser oscillation condition.[20,33] Thus sideband oscillation is supported even though there is no steady (or cw) lasing at the line center

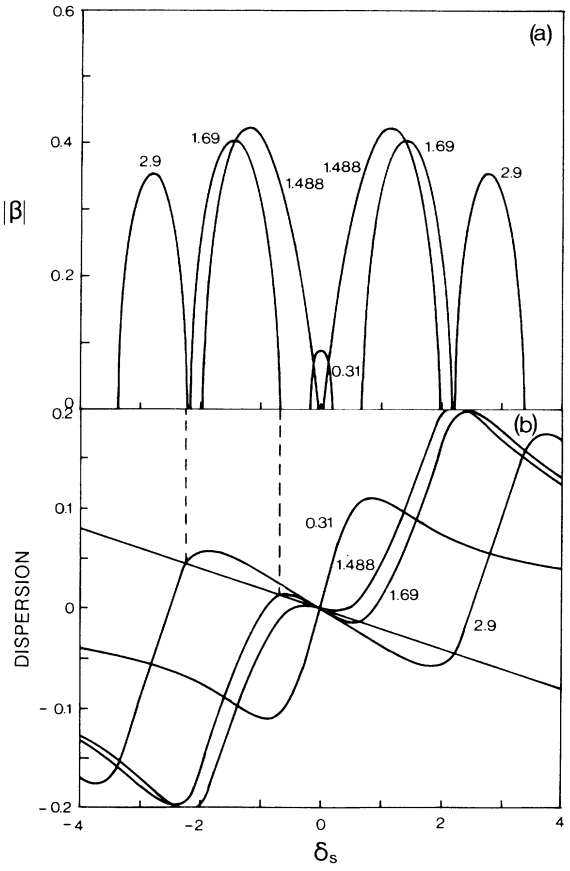

FIG. 4. Variation of the laser emission amplitude β (a) and cavity dispersion (b) with laser signal detuning for $b=0.8$. At $\alpha=0.31$, the laser is above the lasing threshold and the dispersion relation has a single intersection with cavity line at the line center. For $\alpha=1.488$ the center of the emission line drops below the lasing threshold, there are no other intersections of the dispersion curve with the cavity line, and cw lasing ceases. When the pump is further increased to $\alpha=1.69$, two additional intersections of the dispersion curve with cavity line move under the "Rabi-split" gain curve. The laser sees gain at these sideband frequencies and emits stable Rabi oscillations. Increasing the pump beyond $\alpha=2.9$ moves the sideband frequencies outside the gain lobes terminating the oscillations.

because the center-line gain is below threshold. The termination of the Rabi sideband branch at HB2 coincides with the point at which the cavity line and dispersion curve intersections move outside the gain lobes so that the sideband frequencies have no net gain. We remind the reader that this mode-splitting picture is valid strictly only in the perturbation limit of weak lasing emission.[34] It serves the important purpose of allowing us to associate the nonlasing branch of period solutions with pump-induced Rabi sideband oscillations.

An interesting situation is reached at $b=0.7$ [Fig. 2(c)] where the Hopf bifurcation point HB1 is very nearly coincident with the pitchfork bifurcation point BP2. This indicates the existence of a codimension-2 bifurcation,[35] the implications of which remain to be investigated. For values of $b<0.7$, the distribution of bifurcation points is significantly different. The diagram for $b=0.6$ [Fig. 2(d)] shows a symmetrically disposed pair of Hopf bifurcation points on the steady-state lasing branches. In contrast to the subcritical Hopf bifurcation points of the Lorenz-Haken model marking the onset of chaotic behavior in that model, these Hopf bifurcations are supercritical. The branches of periodic solutions emanating from these mirror-image Hopf bifurcations are mathematically and physically distinct from the branch of pump-induced Rabi sideband oscillations originating at HB2. We identify these bifurcations with the usual Haken second lasing threshold and the periodic solutions with *sustained* relaxation oscillations in the laser (only the positive-β HB1 branch is indicated in the figure). The coherent effects that lead to the second lasing threshold of the Lorenz-Haken system can be pictured as involving both field-atom energy relaxation oscillations and Rabi oscillations on the lasing transition. In two-level systems such oscillations are produced by the lasing field alone. In the three-level OPML, the additional and significant contribution of the pump to Rabi oscillation is responsible for the difference in bifurcation and dynamical behavior. For $b=0.8$, the single branch of pump-induced Rabi oscillations was always stable. In this case, both the Rabi oscillation branch and the two mirror-image sustained relaxation oscillation branches eventually lose stability. For $b=0.6$, however, at least one stable stationary or stable periodic solution exists for every pump parameter value and therefore we can expect no long-term chaotic behavior.

The bifurcation diagram for $b=0.2$ exhibits the same qualitative features described above with distinct branches of periodic solutions emanating from HB1 and HB2. An enlargement of part of the bifurcation diagram near HB1 is shown in Fig. 5. The branch of sustained relaxation oscillations originating at HB1 manifests itself as a periodic modulation of a cw lasing emission. Along this branch, the amplitude of this modulation grows with increasing α until a limit point is encountered ($\alpha=0.905$), at which point the branch turns around and the limit cycle associated with it becomes unstable. The loss of stability of the Rabi sideband oscillations below $\alpha=1.145$ indicates the existence of a narrow pump parameter window ($0.905<\alpha<1.145$) in which no stable fixed point or limit cycle exists. The dynamics of this region are chaotic with the distinct geometric features of both limit cycles reflected in the chaotic attractor topology. This point will be addressed further in Sec. III. For pump parameter values in the region immediately below HB1, unstable limit cycles of all branches coexist with the stable sustained relaxation oscillations. This coexistence indicates the possibility of long chaotic-type transients to the stable limit cycle depending critically on the initial state of the system.

The bifurcation diagrams presented in Fig. 2 illustrate the trends in steady-state and oscillatory operating characteristics of an OPML under a two-parameter variation. In contrast to the Lorenz-Haken system which possesses a single pitchfork point, the OPML model ex-

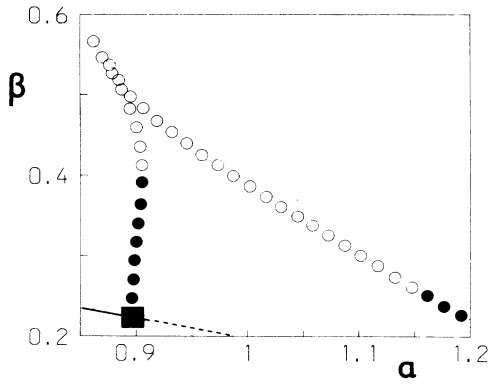

FIG. 5. Enlargement of the bifurcation diagram for $b=0.2$ in the vicinity of the chaotic window. The maximum amplitudes of stable and unstable limit cycles are marked by closed and open circles, respectively.

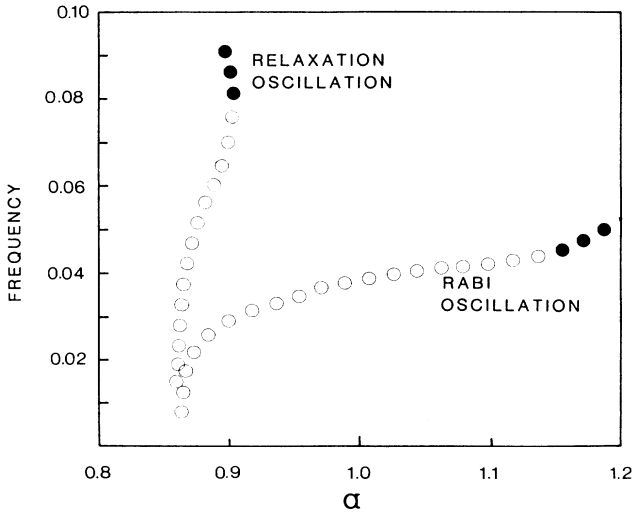

FIG. 6. Plot of the frequency of the two branches of periodic solutions (relaxation type from HB1 and Rabi type from HB2) for $b=0.2$ in the vicinity of the chaotic region. Stable and unstable limit cycles are marked by closed and open circles, respectively.

hibits a pair of such points, between which steady-state lasing branches exist. In the OPML system, as in the Lorenz-Haken system, Hopf bifurcations can occur on the lasing branches, but they are supercritical rather than subcritical, leading to sustained relaxation oscillations rather than chaotic lasing. The significant new dynamical feature to emerge is the separate branch of pump-induced Rabi sideband oscillations emanating from Hopf bifurcations on the nonlasing stationary solution branch.

III. GLOBAL DYNAMICS BEHAVIOR

In this section we discuss the global dynamical aspects of the OPML prompted by the local information of the preceding bifurcation analysis. A clear distinction can be drawn between the lasing emission characteristics associated with the two physical mechanisms of sustained relaxation oscillation and pump-induced Rabi sideband oscillation (hereafter referred to as Rabi oscillation). We confine our study to the bifurcation diagram for $b=0.2$ and to the vicinity of the anticipated chaotic window ($0.905<\alpha<1.145$).

Figure 6 shows the sustained relaxation oscillation and Rabi oscillation frequencies for pump laser magnitudes spanning the window. The sustained relaxation oscillation frequency which is a maximum at the Hopf bifurcation point HB1, decreases along the periodic branch to a value of 0.08 at the limit point ($\alpha=0.905$). Beyond this point the limit cycle is unstable and its frequency decreases rapidly (the period increases). The frequency of the Rabi oscillation, which is unstable for $\alpha<1.145$, decreases gradually across this parameter window and then falls rapidly to zero. The reader should note that the Rabi frequency in this range of α does not correlate with the mode-splitting picture; in fact, there are no new sideband intersections with the cavity line until $\alpha=1.25$. However, for larger values of α beyond the range in this figure, the computed and predicted sideband frequencies converge quickly.

The relative disposition of the two branches in Fig. 6 and their stability properties suggests possible unstable dynamical behavior of the laser, where both physical mechanisms may contribute with different relative weightings. The dynamic characteristics associated with the two physical processes are quite different as shown in Fig. 7, where the amplitude $\beta(t)$, and intensity $\beta^2(t)$, time series are displayed in composite plots. Stable sustained relaxation oscillation manifests itself in amplitude and intensity as a finite amplitude modulation of a nonzero level. For $\alpha=0.902$, the positive amplitude oscillation is shown (dashed line) together with the intensity (solid line). The Rabi oscillation is quite different occurring as a symmetric oscillation about $\beta=0$, as shown for $\alpha=1.18$. The intensity oscillates at twice the frequency of the amplitude. Time series from both extremities of the chaotic window are shown for $\alpha=0.908$ and 1.14. While both signals are chaotic, the predominance of each type of oscillation is evident within each time series. Unstable relaxation-type oscillations occur frequently in the time series for $\alpha=0.908$, reflecting the nearby unstable limit cycles within each half of the β plane ($\beta<0$ and $\beta>0$). Random flips between individual β lobes are relatively infrequent (similar to the Lorenz case). In contrast, the time series for $\alpha=1.14$ shows a predominance of unstable Rabi-type oscillations associated with the topologically different unstable limit cycle. Amplitude excursions within individual β lobes are much less frequent. The chaotic motions on the attractor for $\alpha=0.908$ therefore exhibit infrequent phase switches while those on the attractor for $\alpha=1.14$ switch phase much more frequently.

The computed Lyapunov exponents for a range of α spanning the chaotic window are shown in Table I. They suggest a weakly chaotic motion on a near-flat attractor with strong contraction in four of the six dimensions.

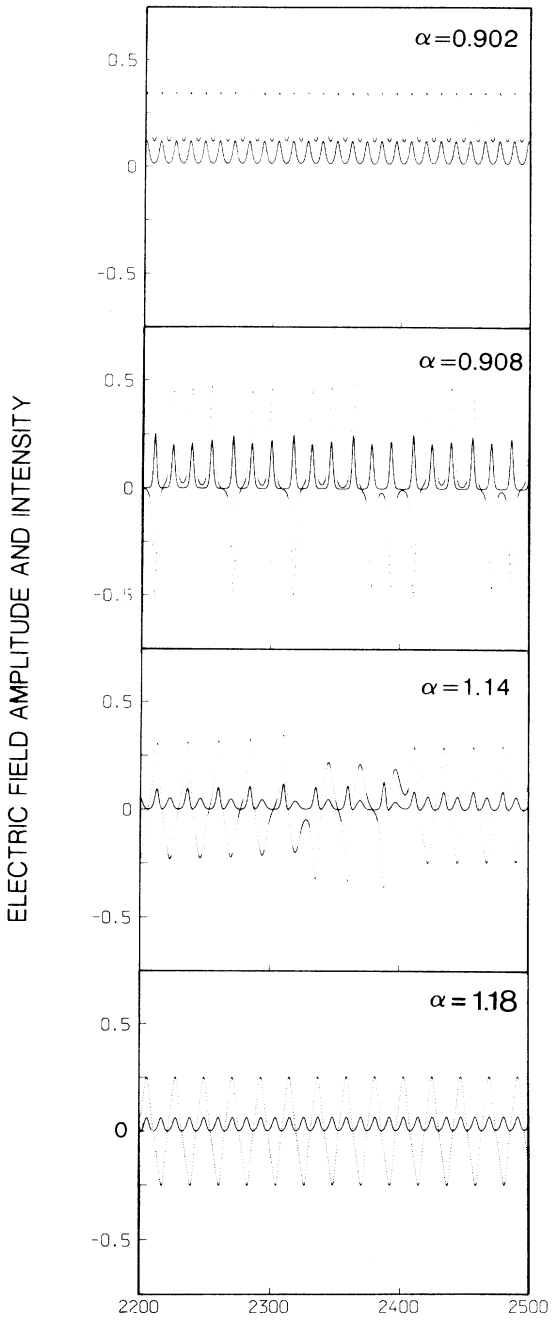

FIG. 7. Representative time series of the laser field amplitude (dotted lines) and intensity (solid lines) for $\alpha=0.902$, 0.908, 1.0, 1.14, and 1.18.

The single positive Lyapunov exponent decreases in magnitude as α is increased across the chaotic window, indicating a greater regularity to the dynamic motion on the attractor.

IV. POWER SPECTRAL ANALYSIS

Our purpose here is to demonstrate the importance of amplitude rather than intensity detection to the study of

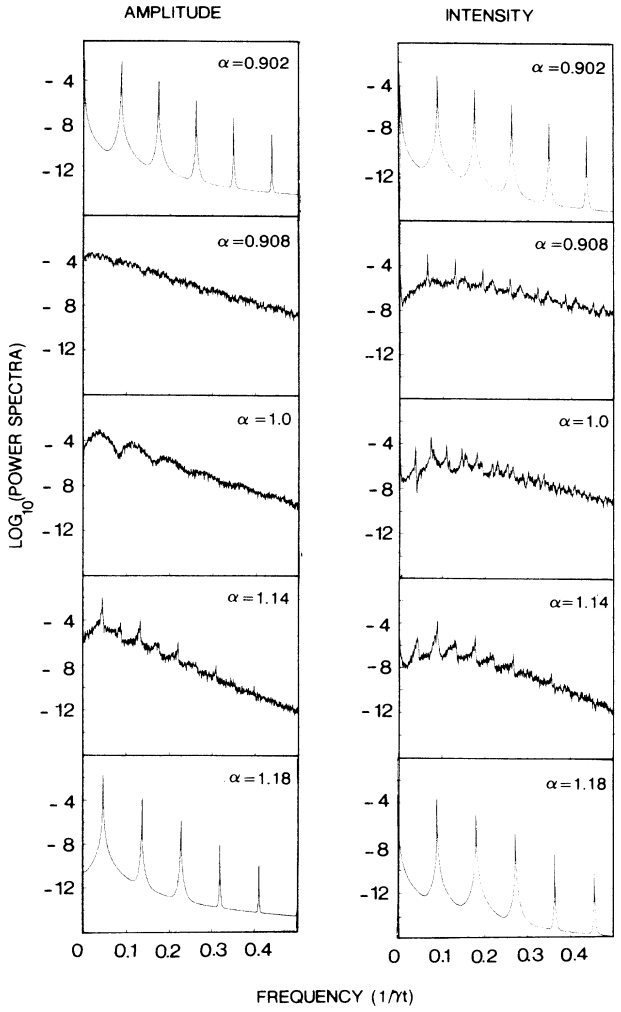

FIG. 8. Power spectra of laser field amplitude and intensity for $\alpha=0.902$, 0.908, 1.0, 1.14, and 1.18.

complex dynamical signals from laser experiments. The chaotic field amplitude time series of Sec. III for $\alpha=0.908$, shows the dynamical motion to be comprised of reasonable regular amplitude excursions interspersed with random phase switches of the field. The corresponding intensity time series supresses this important phase information introducing an artificial semblance of order to the dynamics. Heterodyne detection methods, though experimentally more elaborate, retain this vital phase information. These techniques have been discussed recently in the context of distinguishing between symmetric and asymmetric periodic behavior of the Lorenz-Haken model.[3] Elsewhere, heterodyne spectral analysis has been adopted as a standard experimental and theoretical tool.[36,37] We show here that heterodyne spectra can discriminate between dynamical signals associated with the two distinct physical oscillations of the OPML, whether these signals are periodic or chaotic.

Figure 8 displays amplitude and intensity power spec-

TABLE I. Lyapunov spectra for various values of α spanning the chaotic window for $b=0.2$. The Lyapunov exponents are computed by integration of the OPML equations of motion and the linearized equations over approximately 1000 orbits.

α	λ_1	λ_2	λ_3	λ_4	λ_5	λ_6
0.85	0.0	0.0	−0.85	−0.85	−1.12	−16.49
0.89	0.0	0.0	−0.85	−0.85	−1.12	−16.49
0.902	0.02	0.0	−0.85	−0.85	−1.08	−16.54
0.905	0.06	0.0	−0.84	−0.84	−1.01	−16.67
0.92	0.055	0.0	−0.84	−0.84	−0.95	−16.67
0.945	0.04	0.0	−0.85	−0.85	−0.95	−16.71
0.98	0.03	0.0	−0.85	−0.85	−0.89	−16.75
1.00	0.03	0.0	−0.85	−0.85	−0.86	−16.78
1.05	0.03	0.0	−0.78	−0.85	−0.85	−16.85
1.1	0.04	0.0	−0.78	−0.69	−0.86	−16.94
1.12	0.035	0.0	−0.64	−0.86	−0.86	−16.98
1.14	0.025	0.0	−0.59	−0.86	−0.86	−17.02
1.16	0.0	−0.02	−0.53	−0.86	−0.86	−17.04
1.2	0.0	−0.11	−0.35	−0.86	−0.86	−17.12

tra of time series for a range of pump parameter values α. A number of distinctive features are immediately evident on comparing amplitude and intensity power spectra at fixed values of α. At $\alpha=0.902$, corresponding to sustained relaxation oscillations (periodic modulation of a nonzero level), both power spectra yield the same information. The fundamental frequency corresponds to the point at $\alpha=0.902$ on the relaxation oscillation curve in Fig. 6 and higher harmonics indicate the strong distortion of the relaxation oscillation form from a simple sinusoid.

The broad-band chaotic power spectra for $\alpha=0.908$ are significantly different. The amplitude spectrum is essentially broad band whereas the intensity power spectrum exhibits strong spectral features; similar differences in field amplitude and intensity spectra have been noted for the Lorenz-Haken model.[37] As mentioned above the random switches in phase are an important feature of the dynamics in this case. This information is suppressed in the intensity time series and the sharp spectral features of the intensity power spectrum reflect the artificial regularity imposed on the dynamics. The chaotic power spectra in the middle of the chaotic window at $\alpha=1.0$ again show distinctive characteristics. The amplitude power spectrum now shows spectral features but the intensity spectrum indicates much more regular oscillations. Nearing the end of the chaotic window the power spectra acquire stronger spectral peaks indicating a significant degree of regularity in the laser oscillations. Both amplitude and intensity power spectra for $\alpha=1.14$ confirm the predominance of unstable Rabi oscillation seen in the corresponding time series of Fig. 7.

A marked distinction is observed between the amplitude and intensity power spectra of the stable Rabi oscillation shown for $\alpha=1.18$. The lowest spectral peak in the intensity power spectrum appears at twice the fundamental frequency of the amplitude spectrum. This is to be expected from the corresponding time series in Fig. 7. Confusion can arise, however, when attempting to interpret the physical origin of the laser oscillation. The in-

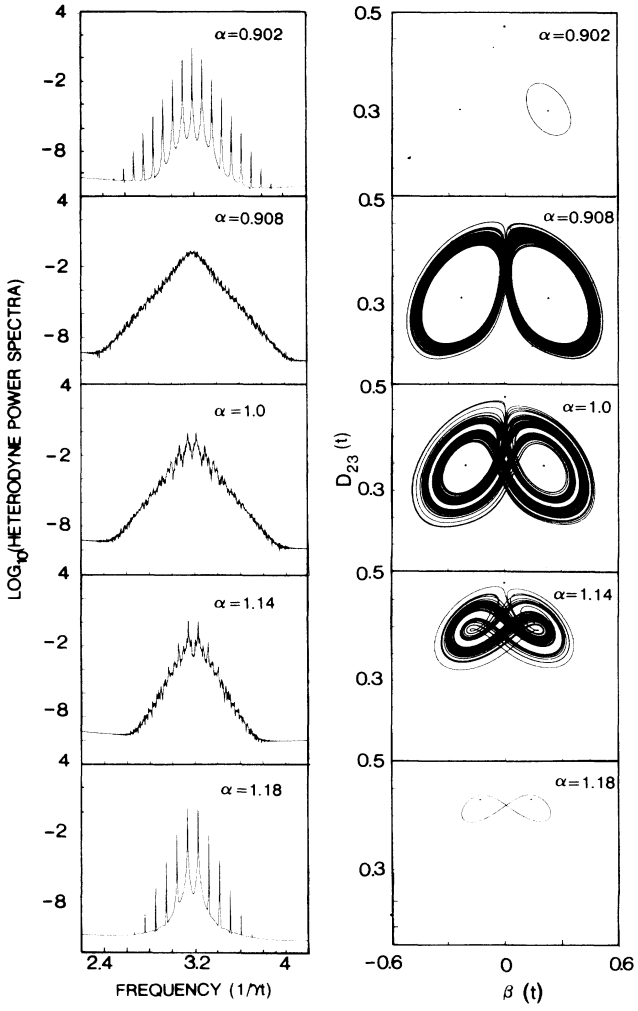

FIG. 9. Heterodyne power spectra and 2D (two-dimensional) phase portraits (D_{23} vs β) for $\alpha=0.902$, 0.908, 1.0, 1.14, and 1.18. The frequency offset between the local oscillator and the lasing field is $10/\pi$ (approximately 3.18) normalized frequency units. The stars on the phase portraits mark projections of the unstable stationary solutions onto the (β, D_{23}) plane.

tensity power spectra at $\alpha=0.902$ and 1.18 look essentially the same, and taken together, this pair could suggest the same dynamic phenomenon with perhaps a small frequency shift due to parameter variation. This near coincidence of the intensity power spectral peaks occurs because the Rabi oscillation frequency is approximately one-half the relaxation oscillation frequency (see Fig. 6). It is possible to envisage how examination of such intensity power spectra could lead to incorrect physical interpretation of experimental data.

Figure 9 shows the heterodyne power spectra of the laser field amplitude with accompanying (β, D_{23}) phase portraits of the corresponding attractors. The heterodyne spectrum for $\alpha=0.902$ has a central peak at the reference frequency of 3.18 indicating that the underlying limit cycle is asymmetric in β. A single sustained relaxation oscillation limit cycle is shown in the phase portrait alongside; the mirror-image (in β) limit cycle coexistent with it is not shown here, but may be accessed from a different set of initial conditions. In contrast, the heterodyne power spectrum shown for $\alpha=1.18$ shows no spectral peaks at the reference frequency; a signature of the symmetric stable Rabi oscillations shown in the corresponding phase portrait. The chaotic attractor for $\alpha=0.908$ is characterized by predominant unstable relaxation oscillations with relatively infrequent switches between the positive and negative β lobes. Across the chaotic window at $\alpha=1.0$ and 1.14, the attractors feature increasing spiraling away from unstable Rabi oscillations with less frequent cycles within individual β lobes. As expected, the chaotic heterodyne power spectra show the same signatures as the corresponding amplitude power spectra discussed previously. Thus, the broad-band and featureless power spectrum for $\alpha=0.908$ acquires increasingly pronounced spectral peaks indicating a regularization of the chaotic motion as α is increased.

V. CONCLUSION

To summarize, results of a theoretical analysis of a single-mode optically pumped molecular laser have been presented for the specific case of resonant pumping and resonant emission. The operating characteristics of the laser are critically dependent on the ratio of the deenergization rate to the dipole dephasing rate. The dynamical behavior of the system is significantly different from that of the equivalent two-level Lorenz-Haken system, due to the coherent interaction of the pump and lasing emission fields. This is manifest through the existence of two distinct forms of limit cycle behavior identified as arising from normal relaxation oscillations and pump-induced Rabi splitting. Finally, we have demonstrated that heterodyne techniques should prove useful in discriminating between laser signals associated with these two physical mechanisms, whether they be periodic or chaotic.

ACKNOWLEDGMENTS

This work was supported by the Science and Engineering Research Council (United Kingdom).

[1]T. H. Maiman, Nature **187**, 493 (1960).
[2]H. Haken, Phys. Lett. **53A**, 77 (1975).
[3]L. M. Narducci, M. Sadiky, L. A. Lugiato, and N. B. Abraham, Opt. Commun. **55**, 370 (1985).
[4]L. W. Casperson, in *Laser Physics*, Vol. 182 of *Lecture Notes in Physics*, edited by J. D. Harvey and D. F. Walls (Springer-Verlag, Berlin, 1983), p. 88.
[5]J. Opt. Soc. Am. B **2**, 1–272 (1985) (special issue on instabilities in active optical media).
[6]J. R. Ackerhalt, P. W. Milonni, and M. L. Shih, Phys. Rep. **128**, 205 (1985).
[7]R. G. Harrison and D. J. Biswas, Prog. Quant. Electron. **10**, 147 (1985).
[8]H. Haken, *Light, Vol. 2, Laser Light Dynamics* (Amsterdam, North-Holland, 1985).
[9]*Instabilities and Chaos in Quantum Optics*, Vol. 34 of *Springer Series in Synergetics*, edited by F. T. Arecchi and R. G. Harrison (Springer-Verlag, Berlin, 1987).
[10]*Optical Instabilities*, Vol. 4 of *Cambridge Studies in Modern Optics*, edited by R. W. Boyd, M. G. Rayner and L. M. Narducci (Cambridge University Press, Cambridge, England, 1986), pp. 249–276.
[11]*Lasers and Synergetics*, Vol. 19 of *Springer Proceedings in Physics*, edited by R. Graham and A. Wanderlin (Springer-Verlag, Berlin, 1987).
[12]J. Opt. Soc. Am. B **5**, 876–1215 (1988) (special issue).
[13]*Instabilities and Chaos in Quantum Optics II*, edited by N. B. Abraham, F. T. Arecchi, and L. A. Lugiato (Plenum, New York, 1988).
[14]N. B. Abraham, P. Mandel, and L. M. Narducci, in *Progress in Optics XXV*, edited by E. Wolf (Elsevier, Amsterdam, 1988).
[15]R. L. Panock and R. J. Temkin, IEEE J. Quant. Electron. **QE-13**, 425 (1977).
[16]T. Heppner, C. O. Weiss, U. Hubner, and G. Schinn, IEEE J. Quant. Electron. **QE-16**, 392 (1980).
[17]S. C. Mehendale and R. G. Harrison, Phys. Rev. A **34**, 1613 (1986).
[18]T. C. Ryan and N. M. Lawandy, IEEE J. Quant. Electron. **QE-22**, 2075 (1986).
[19]M. A. Dupertuis, R. R. E. Salomaa, and M. R. Siegrist, IEEE J. Quant. Electron. **QE-23**, 1217 (1987).
[20]J. S. Uppal, R. G. Harrison, and J. V. Moloney, Phys. Rev. A **36**, 4823 (1987).
[21]M. A. Dupertuis, R. R. E. Salomaa, and M. Siegrist, Opt. Commun. **55**, 370 (1985).
[22]S. C. Mehendale and R. G. Harrison, Opt. Commun. **60**, 257 (1986).
[23]J. Pujol, R. Vilaseca, R. Corbolan, and F. Laguarta, Int. J. Infrared Millimeter Waves **8**, 299 (1987).
[24]J. C. Ryan and N. M. Lawandy, Opt. Commun. **64**, 54 (1987).
[25]J. V. Moloney, J. S. Uppal, and R. G. Harrison, Phys. Rev. Lett. **59**, 2868 (1987).
[26]P. A. Khandokhin, Ya. I. Khanin, and I. V. Koryukin, Opt. Commun. **65**, 367 (1988).
[27]J. Pujol, F. Laguarta, R. Vilaseca, and R. Corbolan, J. Opt. Soc. Am. B **5**, 1004 (1988).
[28]C. O. Weiss and J. Brock, Phys. Rev. Lett. **57**, 2804 (1986).
[29]M. P. Sassi, N. Barbeau, and C. O. Weiss, Appl. Phys. B **43**, 179 (1987).

[30]A. Wolf, J. B. Swift, H. L. Swinney, and J. A. Vastano, Physica **16D**, 285 (1985).

[31]M. Sargent III, M. O. Scully, and W. E. Lamb, *Laser Physics* (Addison-Wesley, New York, 1974).

[32]AUTO: Software for continuation and bifurcation problems in ordinary differential equations, Eusebius Doedel.

[33]S. T. Hendow and M. Sargent III, J. Opt. Soc. Am. B **2**, 84 (1985).

[34]J. S. Uppal, R. G. Harrison, and J. V. Moloney, Opt. Commun. **64**, 357 (1987).

[35]J. Guckenheimer and P. Holmes, *Nonlinear Oscillations, Dynamical Systems and Bifurcations of Vector Fields* (Springer-Verlag, Berlin, 1983).

[36]M. F. H. Tarroja, N. B. Abraham, D. K. Bandy, and L. M. Narducci, Phys. Rev. A **34**, 3148 (1986).

[37]N. B. Abraham, A. M. Albano, B. Das, and M. F. H. Tarroja, in *Fundamentals of Quantum Optics II,* Vol. 282 of *Lecture Notes in Physics* (Springer-Verlag, Berlin, 1987), p. 32.